Steering Characteristics of a Rigid Wheel for Exploration on Loose Soil

Kazuya Yoshida
Dept. of Aeronautics and Space Engineering
Tohoku University
Aoba 01, Sendai, 980-8579, Japan
Email: yoshida@astro.mech.tohoku.ac.jp

Genya Ishigami
Dept. of Aeronautics and Space Engineering
Tohoku University
Aoba 01, Sendai, 980-8579, Japan
Email: ishigami@astro.mech.tohoku.ac.jp

Abstract— In this paper, steering characteristics of a rigid wheel (tire) on loose soil is investigated. Based on terra-mechanics analysis, the lateral force characteristics of a driving wheel is modeled as a function of slip ratio and slip angle. The model suggests that the lateral force decreases according to the increment of the slip ratio and increases according to the increment of the slip angle. Such characteristics are confirmed and evaluated by experiments using simulated lunar-surface soil, called Lunar Regolith Simulant. The proposed model is validated with the experimental results in reasonable precision. A model that properly predicts the lateral force will be useful for future practical issues, such as controlling the steering motion of a vehicle for following a desired trajectory in the operational phase, and also to compare the feasibility and/or stability of candidate steering maneuvers in the motion planning phase.

I. INTRODUCTION

The use of a mobile robot, or *Rover*, for lunar/planetary mission significantly increases the flexibility of exploration, thereby bringing more scientific discoveries [1]. Such a lunar/planetary rover is however expected to travel at a long distance and perform complex scientific tasks. The last decade has seen a considerable amount of research effort in the development of lunar/planetary rovers from various aspects accordingly [2]-[6].

The soil of terrain of a plant is often loose. Intensively studied in the modeling of a wheel is thus a physics-based model, which incorporates traction mechanics between the wheel and terrain as well as the conventional terra-mechanics model. The effect of the traction mechanics of the rover performance in simulation, plan, and control can be found in a number of papers [7]-[14]. Iagnemma et al. [9], for instance, developed an on-line method to identify terra-mechanics parameters of soil (friction angle and cohesion stress) using onboard sensory data. Grand et al. [10] developed a sophisticated simulation model that takes the flow of loose soil under the wheel into account. The present authors [11]-[15] also investigated the wheel-soil traction mechanics by incorporating *slip ratio* as a key parameter for the evaluation of the net traction force, *Drawbar Pull,* on loose soil such as *Lunar Regolith Simulant.*

On loose soil, wheels are easy to slip or spin, then lose traction. The soil under the slipping wheel is removed so that the wheel sinks into the soil. The traction force under the wheel is then subject to the characteristics of this soil removal, which is modeled by the soil's terra-mechanics parameters such as the friction angle and cohesion stress. In addition, *dynamic sinkage* of a spinning wheel is a significant factor to increase the rolling resistance and decrease the net traction of the wheel. It, however, turned out that the traction mechanics including the dynamic effects could be modeled as a function of the slip ratio when the soil and wheel parameters are given.

One remaining concern for the present authors is the modeling of the lateral (side) force of the wheel. When a wheel steers from its traveling direction, lateral force is produced. For pneumatic tires on a rigid surface their steering characteristics have been well studied, though, the study of the steering characteristics for rigid wheels on loose soil that is still an open issue. If the lateral force can be modeled properly, such a model must be useful to control the steering motion of a vehicle to follow a given trajectory. In additionally, the model is used to evaluate and compare possible steering maneuvers from the viewpoint of whether they are feasible and/or stable to follow in the motion planning phase.

In this paper, a physical traction model of a rigid wheel is derived. After enabling the derivation of the longitudinal traction force, the lateral force, which is produced by the shear stress of the soil under the wheel and the *bulldozing resistance* at the sideward of the wheel, is also formulated. The direction of the lateral force is perpendicular to the wheel spin, though, the magnitude of the lateral force has a relationship with the longitudinal slip ratio. As an extreme case, when the longitudinal slip ratio is one (at which the vehicle's traveling velocity is zero, while the wheel is spinning), the lateral force becomes zero.

In order to confirm the model, experiments are carried out using a single-wheel test bed. In the test bed, forces and moments produced by a single wheel are measured when the wheel is forced to travel at an arbitrarily given velocity, given a rotational velocity and a slip angle. Through the experiments, the validity of the developed model is confirmed in the evaluation of the traction forces with a reasonable precision.

The following section presents the definition of wheel coordinate and some symbols. Section III refers to the traction model and particularly deals with the derivation of
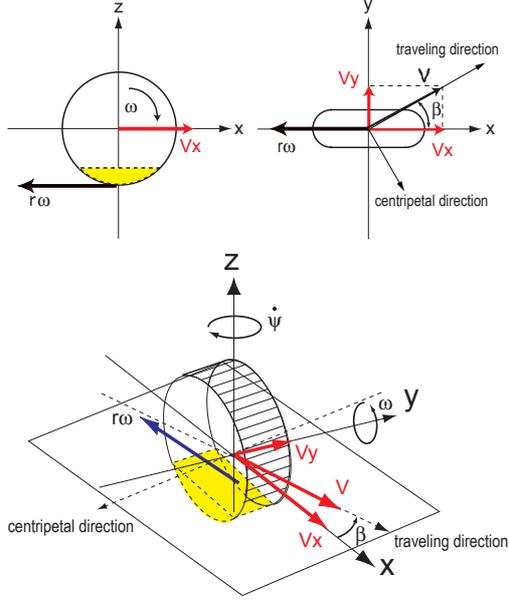
Fig. 1. Definition of the wheel coordinate frame

Fig. 2. Forces and stresses acting on the wheel
(wheel steering towards right)

lateral force. Numerical simulation and experiments results are respectively described in Section IV and V so as to discuss about the proposed traction model.

II. DEFINITIONS AND NOTATIONS

The following analysis deals with a rigid wheel rotating on a loose soil. First, let us define a coordinate system to describe the motion of the wheel using a right-hand frame as shown in Fig.1, where the longitudinal direction is denoted by x, the lateral direction by y, and the vertical direction by z. The coordinate frame turns according to the steering action of the wheel (the yaw rotation around z axis) but does not rotate with the driving motion of the wheel (the pitch rotation around y axis).

The symbols are defined as follows:

ω : angular velocity of the wheel drive (around y axis)
r : radius of the wheel
$r\omega$: circumference velocity of the wheel
β : slip angle
V : traveling velocity of the wheel
V_x : longitudinal traveling velocity ($= V \cos \beta$)
V_y : lateral traveling velocity ($= V \sin \beta$)
F_x, F_y, F_z: forces acting from the ground to the wheel

The angle β, which is called "slip angle," is the angle between the wheel driving direction and its traveling direction. When a vehicle is under the steering action, wheels are making side slip or skidding. This means that wheels have some slip angles.

III. TRACTION MODEL FOR A SINGLE WHEEL

A. Slip ratio and slip angle

When a wheel is traveling on a loose soil, the wheel can slip both in longitudinal and lateral directions. The slip in the longitudinal direction is measured by "slip ratio,"
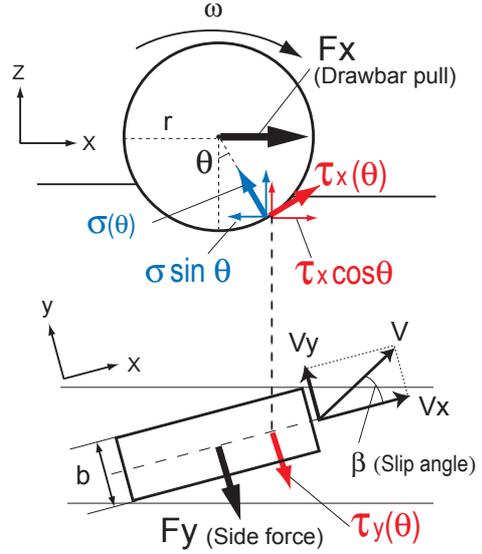
which is defined as a function of the longitudinal traveling velocity and the circumference velocity of the wheel:

$$s = \begin{cases} (r\omega - V_x)/r\omega & (r\omega > V_x : \text{driving}) \\ (r\omega - V_x)/V_x & (r\omega < V_x : \text{braking}) \end{cases} \quad (1)$$

The slip ratio takes a value from -1 to 1.

On the other hand, the slip in the lateral direction is measured by "slip angle," which is defined by the longitudinal and lateral traveling velocity of the wheel as follows:

$$\beta = \tan^{-1} \frac{V_y}{V_x} \quad (2)$$

B. Longitudinal wheel force F_x

A general model for a rigid wheel on loose soil is depicted in Fig.2. The longitudinal force F_x that the soil exerts to the wheel is calculated using the normal stress $\sigma(\theta)$ and the shear stress in x direction $\tau_x(\theta)$ of the soil under the wheel by the integral of those from the entry angle θ_f to the exit angle θ_r [16]-[18]:

$$F_x = rb \int_{\theta_r}^{\theta_f} \{\tau_x(\theta) \cos \theta - \sigma(\theta) \sin \theta\} d\theta \quad (3)$$

where b is the width of the wheel.

The normal stress of the soil $\sigma(\theta)$ is modeled as [14][15]:

$$\sigma(\theta) = \sigma_{max}(\frac{\cos \theta - \cos \theta_f}{\cos \theta_m - \cos \theta_f})^n \\ (\text{for } \theta_m < \theta < \theta_f) \quad (4)$$

$$\sigma(\theta) = \sigma_{max} \left[\frac{\cos\{\theta_f - \frac{\theta - \theta_r}{\theta_m - \theta_r}(\theta_f - \theta_m)\} - \cos \theta_f}{\cos \theta_m - \cos \theta_f} \right]^n \\ (\text{for } \theta_r < \theta < \theta_m) \quad (5)$$

where θ_m is the angle of maximum stress, and at this point the maximum stress σ_{max} is modeled by the following
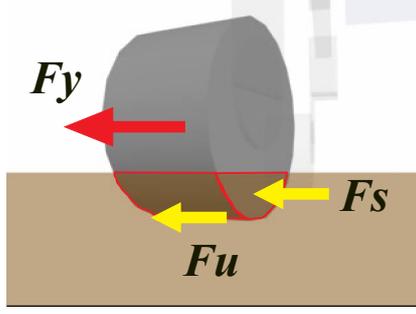
Fig. 3. Lateral (side) forces acting on the wheel (wheel steering towards right)

Fig. 4. Estimation model of bulldozing resistance

terra-mechanics equation [16]:

$$\sigma_{max} = r^n(\frac{k_c}{b} + k_\phi)(\cos\theta_m - \cos\theta_f)^n \qquad (6)$$

The shear stress $\tau_x(\theta)$ is also expressed:

$$\tau_x(\theta) = (c + \sigma(\theta)\tan\phi)[1 - \exp^{-j_x/k_x}] \qquad (7)$$

$$j_x = r[\theta_f - \theta - (1-s)(\sin\theta_f - \sin\theta)] \qquad (8)$$

where the symbols introduced in the equation are represented:

j_x : soil deformation in x direction
c : cohesion stress of the soil
k_c : soil stiffness related to the cohesion
ϕ : internal slip angle of the soil
k_ϕ : soil stiffness related to the friction angle
k_x : shear displacement in x direction

C. Lateral wheel force F_y

The lateral force F_y is given by:

$$F_y = F_u + F_s \qquad (9)$$

where F_u is a force produced by the shear stress in y direction underneath the wheel. F_s is a reaction force generated by bulldozing sideward the wheel as shown in Fig.3.

Derivation of F_u

As shown in Fig.2, the force F_u is subject to the shear stress in y direction $\tau_y(\theta)$. This stress is modeled by the following equation:

$$\tau_y(\theta) = (c + \sigma(\theta)\tan\phi)[1 - e^{-j_y/k_y}] \qquad (10)$$

where k_y is the shear displacement in y direction. The soil deformation in y direction j_y can be calculated by the following equations:

$$
\begin{aligned}
j_y &= \int_0^t V_y dt = \int_\theta^{\theta_f} V\sin\beta\frac{1}{\omega}d\theta \\
&= \frac{V\sin\beta}{\omega}(\theta_f - \theta) \\
&= r(1-s)(\theta_f - \theta)\cdot\tan\beta \qquad (11)
\end{aligned}
$$

Hence, the force F_u is obtained by the integral of $\tau_y(\theta)$ from the angle of contact θ_f to the angle of departure θ_r.

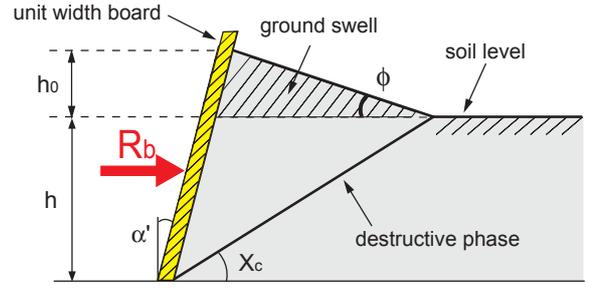$$F_u = rb\int_{\theta_r}^{\theta_f}\tau_y(\theta)d\theta \qquad (12)$$

Derivation of F_s

Hegedus's bulldozing resistance estimation is applied in order to derive the force F_s. As shown in Fig.4, a bulldozing resistance R_b is generated to unit width board when the board moves to the right direction. According to Hegedus's theory, a destructive phase can be assumed as a linear curve, and, moreover, ground swell is considered. Then, the R_b can be estimated as:

$$R_b = \frac{\cot X_c + \tan(X_c + \phi)}{1 - \tan\alpha'\tan(X_c + \phi)} \times$$
$$\left[h\cdot c + \frac{1}{2}\rho h^2\left\{(\cot X_c - \tan\alpha') + \frac{(\cot X_c - \tan\alpha')^2}{\tan\alpha' + \cot\phi}\right\}\right] \qquad (13)$$

In the above equation and in Fig.4, the following symbols are used.

α' : angle of approach
ρ : soil density
h : wheel sinkage
h_0 : height of ground swell
X_c : angle between soil level and destructive phase

Wheel sinkage h is modeled as a function of θ and slip ratio [16]-[18].

$$h(\theta) = r(\cos\theta - \cos\theta_f) + c_0 s \qquad (14)$$

The angle of approach α' should be zero when this estimation is adapted to a case of a sideward of the wheel. Moreover, according to Bekker's theory, the angle X_c can be approximated as described below [18]:

$$X_c = 45° - \frac{\phi}{2} \qquad (15)$$

Thus, adapted R_b is obtained as:

$$R_b = \{\cot X_c + \tan(X_c + \phi)\}\left[h\cdot c + \frac{1}{2}\rho h^2\left(\cot X_c + \frac{\cot^2 X_c}{\cot\phi}\right)\right] \qquad (16)$$

Finally, F_s can be calclated by the integral of R_b from the angle of contact θ_f to the angle of departure θ_r.

$$
\begin{aligned}
F_s &= \int_{\theta_r}^{\theta_f} R_b dl \\
&= \int_{\theta_r}^{\theta_f} R_b(r - h(\theta)\cos\theta)d\theta \\
&= \{\cot X_c + \tan(X_c + \phi)\}\int_{\theta_r}^{\theta_f}\left\{h(\theta) + \frac{1}{2}\rho h^2(\theta)\right. \\
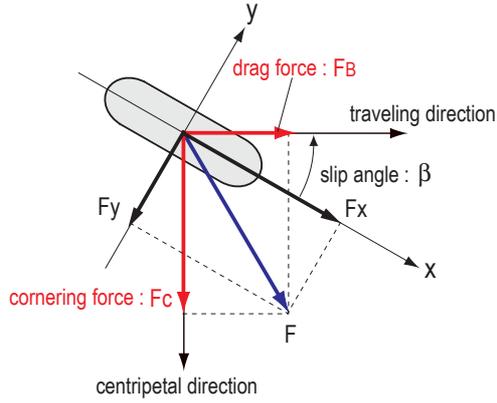&\quad \left.\left(\cot X_c + \frac{\cot^2 X_c}{\cot\phi}\right)\right\}(r - h(\theta)\cos\theta)d\theta \qquad (17)
\end{aligned}
$$

Fig. 5. Geometric relationship for cornering force and drag force (wheel steering towards right)

Fig. 6. Simulation results for the lateral wheel force F_y

Here, dl is an unit width at the sideward of the wheel.

Using equations (9), (12) and (17), the relationship of the lateral wheel force can be obtained as a function of the slip ratio s and slip angle β.

D. Cornering force F_C and drag force F_B

When the wheel is under a steering, the motion of the wheel traces a circular arc. The force in the direction of instantaneous center at the part of the arc is called "cornering force" and denoted by F_C. This force balances with the centrifugal force of a vehicle. On the other hand, the force perpendicular to the cornering force is called "drag force" and denoted by F_B, which balances with the acceleration/deceleration force of a vehicle in the traveling direction. As shown in Fig.5, the relationship of these forces with F_x and F_y is calculated using the slip angle β.

$$F_C = F_x \sin\beta + F_y \cos\beta \qquad (18)$$
$$F_B = F_x \cos\beta - F_y \sin\beta \qquad (19)$$

IV. NUMERICAL SIMULATION

Using the above equations, numerical simulations were carried out to evaluate the lateral force of a wheel and furthermore in order to clarify relationships between the longitudinal and lateral force when other conditions are given.

A. Numerical procedure

The procedure to obtain the wheel forces is summarized as follows:

1) Input the vertical load F_z, the longitudinal slip ratio s, and the slip angle β.
2) Determine the angle of contact θ_f and the angle of departure θ_r from the model of wheel sinkage.
3) Determine the vertical stress $\sigma(\theta)$ and the shear stresses $\tau_x(\theta)$, $\tau_y(\theta)$ under the wheel from the stress distribution model (Equations from (4) to (7)).
4) Determine the longitudinal wheel force F_x by equation (3).
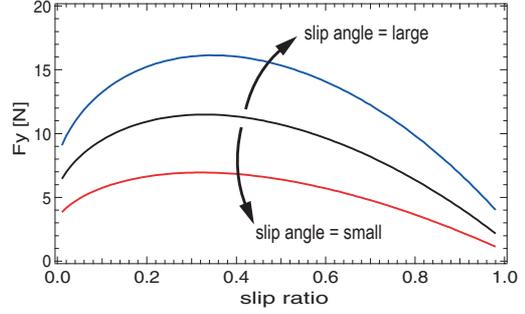5) Determine the lateral wheel force F_y by equations (9).

B. Simulation condition

Simulations were performed under the same condition as the following experiments. For both the simulations and experiments, rigid wheel with a radius of 0.09 [m] and a width of 0.1 [m] was used on a loose soil called "Lunar Regolith Simulant." This is a simulated soil of Lunar Regolith in terms of similar material components and mechanical characteristics.

The parameters used in the simulations are listed in Table.I, the values of which were identified from other experiments. The experiments were carried out based on the terra-mechanics procedure [15].

TABLE I
SIMULATION PARAMETERS AND VALUES

parameter	value	unit
c	0.8	[kPa]
ϕ	37.2	[deg]
r	0.09	[m]
b	0.1	[m]
k_x	4	[m]
k_y	40-50	[m]
k_c	1.79×10^6	[N/m^{n+1}]
k_ϕ	1.95×10^6	[N/m^{n+1}]
c_0	0.031	[m]

C. Simulation result (Lateral wheel force Fy)

Fig.6 depicts an example of simulation results. The figure describes the lateral wheel force F_y as a function of the longitudinal slip ratio s for various slip angles β. From this figure, it is seen that the lateral force approximately has a maximum value at $s = 0.3$, and increases according to the slip angle.

The result is reasonable because the larger the slip angle is the larger the lateral force becomes. It is however interesting to know that the lateral force decreases constantly and finally becomes almost zero at $s = 1.0$.

Note in contrast that the longitudinal force generally increases according to the slip ratio s. At $s = 1.0$, the longitudinal force can be smaller than the value at other slip ratio, but it may not be zero. However, the result of zero lateral force at $s = 1.0$ is quite reasonable from general experiences; when traction wheels start spinning on snowy or icy road, the vehicle loses its steering control.

D. Simulation result (relationship between Fx and Fy)

The Fig.7 shows a relationship between the longitudinal wheel force F_x and the lateral wheel force F_y. According
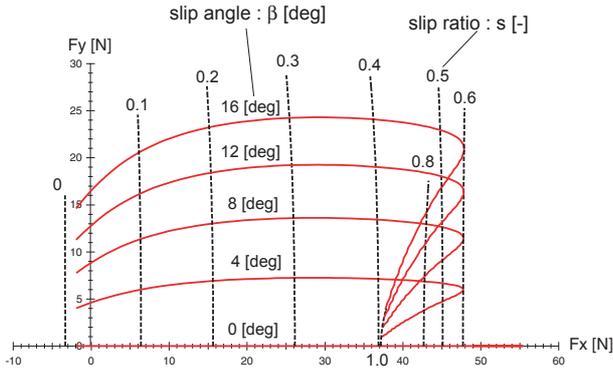
Fig. 7.   relationship between Fx and Fy

Fig. 8.   Single wheel test bed

Fig. 9.   Trace of a wheel on Lunar Regolith Simulant
(wheel steering towards right)

to this graph, when the longitudinal slip ratio s is under a constant state, the longitudinal force is rarely influenced by the slip angle β or the lateral force, while the longitudinal force generally increases according to the slip ratio s as stated previously. However, let us consider that a vehicle steers with a constant value of slip angle β. From Fig.7, when the slip ratio becomes larger than 0.6, the lateral force decreases rapidly in such a case. Then, according to the decrease of the lateral force, the cornering force F_C also reduces as defined in equation (18).

The cornering force is equivalent with the centrifugal force of a vehicle. Hence, drastic decrement of cornering force leads to an instability behavior of vehicles. Particularly, the larger the slip angle, the more easily vehicles will overturn.

Therefore, analyzing the relationship between the longitudinal and lateral force and additionally clarifying the interaction between wheel and soil are important issues in order to discuss about the stability of vehicles including rovers.

V.   Experiments

In order to verify the above simulation results, experiments were carried out using a test bed for a single wheel locomotion.

A. Single wheel test bed

Fig.8 shows the test bed used for the experiments. The test bed is constituted by the wheel traveling and driving units. The wheel traveling unit has a belt conveyer to move the wheel unit with an arbitrary velocity. The wheel is rotated with an arbitrary angular velocity by its driving unit. Arbitrary steering angles (which is equivalent to the slip angle in this case) can be set between the traveling unit and the wheel.

The traveling and rotating velocities are measured by an encoder at the each corresponding driving motor. The wheel forces are measure by a 6-axis force/torque sensor located between the traveling unit and the wheel. Lunar regolith simulant is used for the soil under the wheel.

In the following experiments, the velocities are set so that a longitudinal slip ratio is constant during a single run of the wheel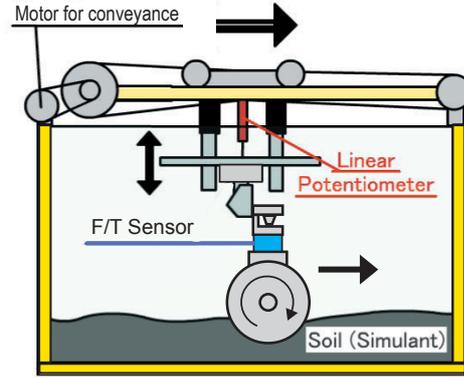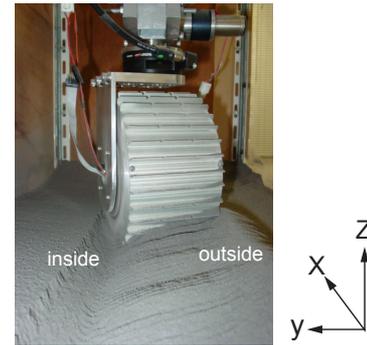 for about 2 meters. The slip ratio is set from 0 to 0.7 with a step of 0.1. The slip angle is also set constant during the single run. The value of the slip angle is set from 0 to 16 degrees with a step of 4 degrees.

B. Experimental results

Fig.9 shows a picture of the trace on the soil after the experiment with the slip angle of 16 degrees and the slip ratio of 0.6. As seen from the picture, the wheel has parallel aluminum fins (paddles) of 1.0 cm height around its surface. Also, it is observed that the trace is not flat but the inside (the centripetal direction) of the wheel is dug deeper than outside. This trend is prominent with larger slip angles.

The lateral force measurements obtained from the experiments are plotted in Figs.10 for each slip angle from 4 to 16 degrees. Corresponding theoretical curve is also drawn in each figure.

Figs.10 confirm the characteristics that the lateral force decreases according to the slip ratio and increases according to the slip angle. The difference of the measured force from the theoretical value is generally very small though, relatively bigger difference is observed in case of 16 degree of slip angle. As mentioned above the trace of the wheel is not flat any more, but the theoretical model introduced in this paper does not consider this effect. This is one of possible reasons for a relatively bigger difference, and this is one of possible points for future improvement of the model.
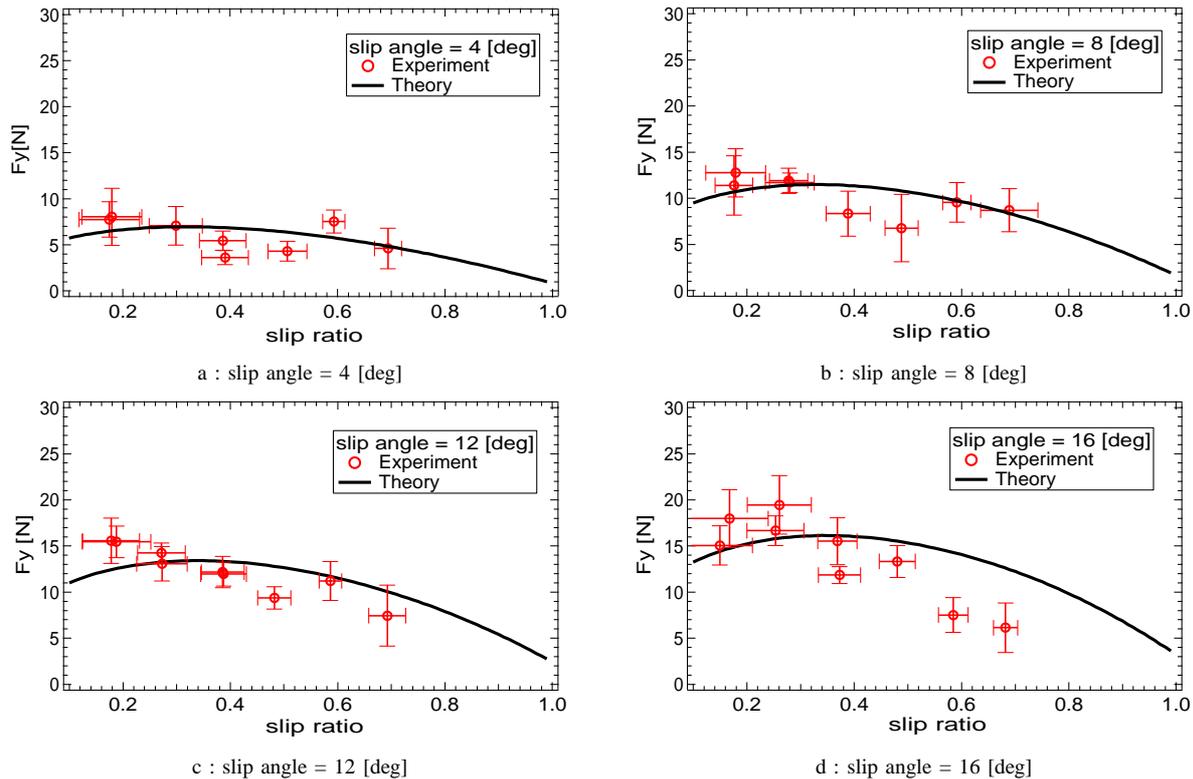
a : slip angle = 4 [deg]

b : slip angle = 8 [deg]

c : slip angle = 12 [deg]

d : slip angle = 16 [deg]

Fig. 10.   Experimental results

VI. Conclusions

In this paper, the steering characteristics of a rigid wheel (tire) on loose soil has been investigated. Based on the terra-mechanics formulation, it was illustrated that a rigid wheel on loose soil has the characteristics that the lateral force approximately decreases according to the slip ratio and increases according to the slip angle. Such characteristics were confirmed and evaluated by the experiments using simulated lunar-surface soil, called Lunar Regolith Simulant. The proposed model was validated with the experimental results in reasonable precision.

The model to properly predict the lateral force will be useful for future practical issues, such as to control the steering motion of a vehicle to follow a given trajectory in the operational phase, and also to compare the feasibility and/or stability of candidate steering maneuvers in the motion planning phase.

References

[1] http://marsrovers.jpl.nasa.gov/home/index.html (as of March 2004)
[2] C.R.Weisbin,et. al.; "Autonomous Rover Technology for Mars Sample Return," *Proc. i-SAIRAS'99,* ESTEC, The Netherlands, June, 1999, pp.1–10.
[3] J.Aizawa, N.Yoshioka, M.Miyata, Y.Wakabayashi; "Designing of Lunar Rovers for High Work Performance," *Proc. i-SAIRAS'99,* ESTEC, The Netherlands, June, 1999, pp.63–68.
[4] Y.Kuroda, K.Kondo, K.Nakamura, Y.Kunii, T.Kubota; "Low Power Mobility System for Micro Planetary Rover *Micro5*," *Proc. i-SAIRAS'99,* ESTEC, The Netherlands, June, 1999, pp.77–82.
[5] M.Tarokh, Z.Shiller, S.Hayati; "A Comparison of Two Traversability Based Path Planners for Planetary Rovers," *Proc. i-SAIRAS'99,* ESTEC, The Netherlands, June, 1999, pp.151–157.
[6] J. Balaram; "Kinematic Observers for Articulated Rovers," *Proc. 2000 IEEE Int. Conf. of Robotics and Automation,* CA, USA, April, 2000, pp.2597–2604.
[7] Farritor, S., Hacot, H., and Dubowsky, S.; "Physics-Based Planning for Planetary Exploration," *Proceedings of the 1998 IEEE International Conference on Robotics and Automation,* 278-283, 1998.
[8] Iagnemma, K., and Dubowsky, S., "Mobile Robot Rough-Terrain Control (RTC) for Planetary Exploration," *Proceedings of the 26th ASME Biennial Mechanisms and Robotics Conference,* DETC 2000.
[9] Iagnemma, K., Shibly, H., Dubowsky, S., "On-Line Traction Parameter Estimation for Planetary Rovers," *Proceedings of the 2002 IEEE Int. Conf. on Robotics and Automation,* pp. 3142–3147, 2002.
[10] C.Grand, F.Ben Amar, P.Bidaud, "A Simulation System for Behaviour Evaluation of Off-road Mobile Robots," *4th International Conference on Climbing and Walking Robots,* Sept. 2001, Germany.
[11] K.Yoshida, H.Asai and H.Hamano, "Motion Dynamics of Exploration Rovers on Natural Terrain: Experiments and Simulation," *Proc. of the 3rd International Conference on Field and Service Robotics,* Finland, 281–286, June, 2001.
[12] K. Yoshida, H. Hamano; "Motion Dynamics of a Rover With Slip-Based Traction Model," *Proc. 2002 IEEE Int. Conf. on Robotics and Automation,* pp.3155-3160, 2002.
[13] K. Yoshida, H. Hamano; "Motion Dynamics and Control of a Planetary Rover With Slip-Based Traction Model," *SPIE 16th Int. Symp. on Aerospace/Defense Sensing, Simulation, and Controls,* SPIE4715-33, 2002.
[14] K. Yoshida, T. Watanabe, N. Mizuno, G. Ishigami; "Terramechanics-Based Analysis and Traction Control of a Lunar/Planetary Rover," *4th Int. Conf. on Field and Service Robotics,* July 2003.
[15] Kazuya Yoshida, Noriyuki Mizuno, Genya Ishigami, Akiko Miwa; "Terramechanics-Based Analysis for Slope Climbing Capability of a Lunar/Planetary Rover" *24th Int. Symp. on Space Technology and Science,* June 2004.
[16] Wong, J. Y., Theory of Ground Vehicles, John Wiley & Sons, 1978, chapter 2.
[17] Bekker, G. M, Introduction to Terrain-Vehicle Systems, The University of Michigan Press, Ann Arbor, 1969.
[18] Bekker, G. M, OFF-THE-ROAD LOCOMOTION, The University of Michigan Press, Ann Arbor, 1960.